Agricultural and Forest Meteorology 269–270 (2019) 57–70

Contents lists available at ScienceDirect

Agricultural and Forest Meteorology

journal homepage: www.elsevier.com/locate/agrformet

Disentangling the formation and evolvement mechanism of plants-induced dried soil layers on China's Loess Plateau

Yuhua Jia[a,*,1], Tongchuan Li[b,1], Ming'an Shao[c,**], Jianhui Hao[a,g], Yunqiang Wang[d], Xiaoxu Jia[b], Ceng Zeng[e], Xiaoli Fu[b], Bingxia Liu[f], Miao Gan[a], Mingyang Zhao[a], Xinni Ju[a]

[a] Shenyang Agricultural University, Shenyang, 110866, Liaoning, China
[b] Key Laboratory of Ecosystem Network Observation and Modeling, Institute of Geographic Sciences and Natural Resources Research, Chinese Academy of Sciences, Beijing, 100101, China
[c] State Key Laboratory of Soil Erosion and Dryland Farming on the Loess Plateau, Institute of Soil and Water Conservation, Northwest A&F University, Yangling, 712100, Shaanxi, China
[d] State Key Laboratory of Loess and Quaternary Geology, Institute of Earth Environment, Chinese Academy of Sciences, Xi'an, 710061, Shaanxi, China
[e] Key laboratory of Tibetan Environment Changes and Land Surface Process, Institute of Tibetan Plateau Research, Chinese Academy of Sciences, Beijing, 100101, China
[f] Key Laboratory of Agricultural Water Resources, Hebei Laboratory of Agricultural Water-Saving, Center for Agricultural Resources Research, Institute of Genetics and Developmental Biology, Chinese Academy of Sciences, Shijiazhuang, 050021, Hebei, China
[g] Inner Mongolia University For The Nationalities, Tongliao, 028000, Inner Mongolia, China

ARTICLE INFO

Keywords:
Soil water resources
Soil drought
Revegetation
Gain for green program
Sandwiched dried soil layer

ABSTRACT

The extent of the effect of China's Loess Plateau on global climate change partially depends on the achievements of the Grain for Green Program (GFGP). This region is prone to drought problems, especially the widespread creation of dried soil layer (DSL), which is intensified by the revegetation from GFGP initiatives. A DSL is the result of soil desiccation in deep soil profiles. The occurrence and expansion of DSLs are strengthened by the high risk of the Loess Plateau to climate change. On the basis of the 14-year data of soil water content (SWC) of four revegetation types on a loessial slope, we investigated the evolution processes and recovery possibility of DSL. Results showed that both variation trends and abrupt changes in the SWC time series were distinctly affected by revegetation. The 40 cm thickness of the DSL was triggered when *Medicago sativa* and *Caragana korshinskii* grew for 2 and 4 years, respectively. The downward extension depth of DSL reached 580 cm under the two plants above within 7 and 8 years of planting. However, the results suggested the possibility of DSL disappearance as shown by the formation depth dynamics of DSL, the fluctuation of DSL-SWC, and the phenomenon of sandwiched DSL. During deep moisture recharge and DSL recovery, although the SWC sensitivity to textural variation was present in the vertical profile, the effects of soil texture on SWC were decreased. Wet climate was linked to both DSL thinning and thickening. Thus, the effect of wet climate is bidirectional for DSL development, thereby highlighting the important role of revegetation. The results of this work enhance our understanding of DSL and may help alleviate the risk of drought in the Loess Plateau.

1. Introduction

China's Loess Plateau, which is the largest and deepest loess deposit in Asia, is characterized by a substantially eroded terrain. Severe soil erosion has sculpted the terrain and created a broken hill and gully landscape, thereby resulting in a fragile regional ecosystem (Fu et al., 2016). As a key engineering strategy for erosion control and vegetation restoration, Grain for Green Program (GFGP) was initiated in 1999. Consequently, the vegetation cover in Loess Plateau almost doubled by 2013, and the area became one of the most prominent ecological restoration zones in China (Fu et al., 2016). However, the unprecedented decline of streamflow and sediment load also occurred (Chen et al., 2015; Liang et al., 2015; Wang et al., 2016). Revegetation increases the net primary productivity (NPP) and evapotranspiration, which results in unexpected water shortage in drought-prone environment. The contributing factors include the fact that the current vegetation cover

* Corresponding author at: College of Water Conservancy, Shenyang Agricultural University, Shenyang, 110866, China.
** Corresponding author at: State Key Laboratory of Soil Erosion and Dryland Farming on the Loess Plateau, Institute of Soil and Water Conservation, Chinese Academy of Sciences and Ministry of Water Resources, Yangling, 712100, Shaanxi, China.
E-mail addresses: jiayuhua@163.com (Y. Jia), shaoma@igsnrr.ac.cn (M. Shao).
[1] Yuhua Jia and Tongchuan Li are the co-first authors.

https://doi.org/10.1016/j.agrformet.2019.02.011
Received 23 August 2018; Received in revised form 1 January 2019; Accepted 6 February 2019
Available online 12 February 2019
0168-1923/ © 2019 Elsevier B.V. All rights reserved.

exceeds the climate-defined equilibrium state (Zhang et al., 2018), and that NPP approaches its threshold defined by water resource sustainability (Feng et al., 2016). This phenomenon was demonstrated by the occurrence and expansion of dried soil layer (DSL).

DSL is a soil desiccation phenomenon that forms below the mean annual infiltration depth and can be induced by the excessive soil water depletion by exotic perennial plants (Chen et al., 2008b; Li, 1983; Shao et al., 2018; Wang et al., 2004b). As a detrimental ecohydrological phenomenon of deep loessial soil, DSL was first observed at a depth of 2.6 m in a high-yield farmland in drought-affected Pucheng and Chengcheng county in 1965 (Li, 1983, 2015). DSL has attracted minimal attention until the 1980′s (Chen et al., 2008a) when it was observed in the upper 5 m of the soil under alfalfa (*Medicago sativa*) grassland in Wugong county and the upper 8 m of soil under the natural forest in Ziwu Mountain (Li, 2015). Similar phenomenon such as deep soil desiccation exists worldwide (Chen et al., 2008b; Green et al., 2006; Jipp et al., 1998; Robinson et al., 2006); however, the DSL of Loess Plateau is the most notable among these phenomena. DSL has a regional distribution over a large area, with a mean thickness of 160 cm and a mean formation depth of 270 cm (Wang et al., 2010a). Shangguan (2007) indicated that DSL is the ecological aftermath of intense soil desiccation due to disturbed plant succession and soil water depletion. Zhang et al. (2018) considered excessive afforestation as the factor primarily responsible for local soil drying. Nevertheless, the elimination of DSL is difficult once it develops large thickness over a large area, and widespread overplanting under increasing drought will worsen soil drying (Zhang et al., 2018). All these findings suggested a compelling need to understand DSL formation and evolvement, as well as its possibility to be recovered.

The feedback from DSL to the ecosystem occurs via multiple mechanisms. When soil moisture approaches the wilting point, DSL restricts normal plant growth and increases the risk of plant mortality and environment degradation (Chen et al., 2008b; Shao et al., 2018; Wang et al., 2001). Evapotranspiration decreases due to the persistent existence of a thick DSL and insufficient available soil water. The amount of soil water replenishment during the rainy season decreases as the wetting front through the soil is impeded by the DSL. Both output and input in water budget are affected by DSL, which alters the watershed hydrology. When the spatial scale is upgraded from the watershed to the entire region, both terrestrial ecosystem services and functions are impaired by the DSL. Thus, the assessment of ecological success by revegetation is negatively affected by the DSL (Chen et al., 2015; Jia et al., 2017; Jiao et al., 2012; Wang et al., 2018a). Given its adverse impacts on revegetation, water resources, and ecosystem services, the DSL in the Loess Plateau is a major ecological problem and focus of research attention in the areas of soil physics, ecohydrology, and agronomy (Shao et al., 2018).

From the perspective of a multimodel ensemble (Samaniego et al., 2018) at a global scale, deep soil profiles must be considered for a comprehensive assessment of climate change, especially for large loess-covered areas. The role of Loess Plateau in global change depends largely on GFGP achievements. By the end of 2008, 96.1 Tg additional C was sequestered from the ecosystem, which resulted in the region changing from a net C source to a net C sink (Feng et al., 2013). Loess Plateau also contributes to climate change through its unique gullied landform across an area of 640,000 km^2, which receives precipitation and shows an increase in the evaporating moisture in gully slopes (Gan et al., 2019). As the stage before DSL, soil desiccation is a consequence of drought and particularly acute in Loess Plateau (Wang et al., 2010a). The interaction between soil desiccation and atmospheric circulation may be related to the interannual variability of the regional climate (Samaniego et al., 2018), especially the increase in seasonal temperature variability (Seneviratne et al., 2006) and extreme heatwaves (Miralles et al., 2014). Therefore, Loess Plateau is expected to contribute to global change by aggravating soil drought and especially, the widespread DSL that is intensified with revegetation.

As an ecohydrological phenomenon and one of the major issues limiting ecosystem sustainability during the process of vegetation restoration, the DSL in Loess Plateau has received considerable attention, and a few excellent reviews on this subject have been published (Chen et al., 2008b; Huang et al., 2003; Li, 1983; Shangguan, 2007; Shao et al., 2016, 2018; Wang et al., 2004a, b; Yan et al., 2015). Although some aspects of the research on DSL, including its negative effect, spatiotemporal distribution, controlling factors, and countermeasures, have been clarified, and many studies have substantially improved our understanding of this topic (Chen et al., 2008a; Jia et al., 2017; Miralles et al., 2014; Wang and Wang, 2018; Wang et al., 2010b, 2011; Wang et al., 2018b), the underlying mechanism responsible for DSL formation is poorly understood, and the possibility of DSL recovery remains uncertain. DSL is an isolated strip for water transfer (Chen et al., 2008b), which prevents water interchange between the upper soil layers and the groundwater (Wang et al., 2011). However, this opinion may be challenged by the lack of direct evidence. Generally, the soil moisture throughout the profile is unmonitored as regularly as temperature or precipitation (Zhou et al., 2011). Previous works regarding the relationship between DSL and the years of plant cultivation, that is, planting years, have primarily used spatial methods instead of temporal sequences (Jia et al., 2017; Wang et al., 2010b; Yan et al., 2015), which cannot fully represent the temporal dynamics of DSL development. Thus, according to a consecutive observation of soil water content (SWC) under revegetation, this study aims to 1) investigate the processes of DSL formation and evolution under perennial deep-rooted plants and 2) test whether plant-induced DSL stops moisture replenishment in the soil profile.

2. Materials and methods

2.1. Study site description

The study site Liudaogou catchment (110° 21′ - 110° 23′ E, 38° 46′ - 38° 51′ N) is located in Shenmu County of Shaanxi Province and covers approximately 7.09 km^2. The catchment has a fragmented terrain and consists of about 38% gully area (Gong et al., 2018). Elevation of the area ranges from 1081 m at the gully bottom to 1273.9 m at the dividing waterline.

The original vegetation has been destroyed by long-term historical soil erosion and human activities which included deforestation, overgrazing and slope farmland creation. Great efforts and effective measures to control the intense soil erosion were taken in the 1980′s: terraces were built or slope farmland was abandoned, check dams were built to trap sediments, and the breeding scale of goats and sheep were downsized (Tang et al., 1993). Followed by vegetation restoration in response to GTGP in 1999, a mosaic distribution (Fu et al., 2012; Wu et al., 2016) of planted forest, grassland and crop cultivation was created, with plant species mainly consisting of *Caragana korshinskii Kom.*, *Medicago sativa*, *Stipa bungeana*, *Salix psammophila*, *Lespedeza davurica*, *Artemisia capillaris*, *Tripolium vulgare*, *Populus simonii*, and *Prunus armeniaca*.

2.2. Experimental design

In 2003, four large plots, each with an area of 500 cm in width and 6100 cm in length, were established on a slope fallow (12-14°, northwestern aspect). The distance between neighboring plots was 90 cm, and the plot borders made of concrete were 10 cm wide and built 30 cm into the ground. The plots correspond to four revegetation types: Korshinsk peashrub (KOP), purple alfalfa (ALF), natural fallow (NAF) and millet (MIL) (Fig. 1). The plots of KOP and ALF represent shrubland and grassland, with plants planted 70 cm and 50 cm apart, respectively. Millet was cultivated in the MIL plot to represent an agriculture.

In 2004, 44 boreholes were made in the four plots (for a total of 11 observations sites in each of the four treatments) using the soil augers

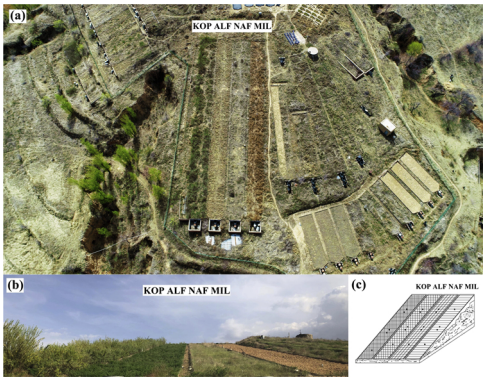

Fig. 1. Experimental plots of the revegetation types of Korshinsk peashrub (KOP), purple alfalfa (ALF), natural fallow (NAF), and millet (MIL). The aerial and ground image labeled as (a) that was taken by DJI Phantom 4 Pro$^+$ on April 9, 2018 shows the bird's eye view of the study area. The image labeled as (b) that was taken on May 11, 2018 demonstrates the vegetation coverage in the early growing season. The planed observational sites installed with neutron-probe access tubes are shown in the image labeled as (c), with three tubes accessing the depth of 580 cm installed in each plot in 2004, and the other tubes accessing the depth of 960 cm installed in 2014.

and neutron tubes were installed to measure SWC using a neutron probe. Among the 11 observational sites in each plot, eight sites had access to the depth of 400 cm, and three sites to the depth of 580 cm. We used the data down to 580 cm depth rather than 400 cm depth during this study. To determine the rates and extent of erosion processes, the four plots originally aimed to exam the ability of revegetation types to control soil erosion (Zeng et al., 2011). With the increase in vegetation age as well as vegetation cover, runoff and sediment induced by heavy rainfall were rarely produced in KOP and ALF. They were suitable for incorporation in consecutive experiments for exploring the relationship between profile soil moisture and revegetation plant selection as shown in previous studies (Fu et al., 2012; Jia et al., 2017; Jia and Shao, 2013, 2014; Jia et al., 2013; Liu and Shao, 2014; Zhao et al., 2017).

Investigation of soil moisture at depths to which plant roots may extend is essential for understanding soil water dynamics, which had a strong buffering capacity to alleviate the effects of seasonal or inter-annual drought on plants (Jipp et al., 1998). Plant roots in plots of KOP and ALF might extend below 580 cm, which was the deepest observational depth before 2014. Allowing for the occurrence of DSL in KOP and ALF plots and the need of observational depths exceeding 580 cm, two new observational sites in each plot of KOP, ALF and NAF, and one new observational site in MIL plot, were added in 2014. A soil auger or Luoyang shovel (Ma et al., 2013) was bolted with extensive handles to bore into deep soil and the calcic nodules were broken into pieces with the help of a custom-made piercer. The neutron tubes were subsequently installed and combined in the deep soil profiles. Such observation deep to a depth of 980 cm was not rare for investigation of soil water resources in the vadose zone (Green et al., 2006; Tye et al., 2011; Zhu et al., 2018).

2.3. Data collection

2.3.1. Climatic parameters

Climatic parameters associated with precipitation, temperature and standardized precipitation evapotranspiration index (SPEI) were considered in an attempt to aid understanding of DSL development over time. The historical daily precipitation and temperature mainly derived from the NOAA website. The climate data of Yulin station (ID: CHM00053646) were used as a substitute for the weather conditions in Shenmu County of Yulin city. Another two sets of precipitaion data for the Liudaogou catchment were used to calculate the average precipitation throughout the study site. One set of the data was recoreded manually, and the other by automatic rain gauge. These two sets of data were not continous or absent of other parameters. Therefore, monthly precipitaion and temperature were acquired based on these data sets.

The amount and frequency of precipitation events of > 10 mm were incorporated. We also added two other associated parameters: antecedent precipitation within 30 days (API) and Cumulative Precipitation Index (CPI). The API refers to the 30-day accumulated precipitaion since an individual reading of SWC. We proposed the CPI in order to compare the cumulative monthly precipitation (CMP) in a certain year with the yearly average of CMP. The CPI is calculated as:

$$CPI_{k,i} = \frac{\sum_{i=1}^{N_i} p_{k,i}}{\frac{1}{N}\sum_{k=1}^{N_k}\sum_{i=1}^{N_i} p_{k,i}} \quad (1)$$

where $CPI_{k,i}$ is the *CPI* for the month i in year k, $P_{k,i}$ is the precipitation for the month i in year k. Specifically, i = 1, 2, …,12, k = 1, 2, …14, and k corresponds to 2004, 2005,…, 2017, respectively. The N_i is the number of months from January to month i in a year. The N_k is the number of years from the 1st year to k. Due to the need for calculating yearly average of CMP, N was assigned a value of 14 to represent the total number of observational years in this study. For CPI, we sought to determine in any month of the same year whether the precipitation amount increased or decreased compared to the whole observational period.

The SPEI data with timescales of 1, 3 and 6 months during the period of 2004–2015 were acquired from the SPEI base (http://sac.csic.es/spei/database.html). The SPEI is designed to take into account both precipitation and potential evapotranspiration when determining drought (Vicente-Serrano et al., 2010) and has been used to characterize climate chaneg in the Loess Plateau (Gao et al., 2017).

2.3.2. Soil texture, fractal dimension and median diameter

We collected disturbed soil samples in the deep soil profile in 2014 at depth intervals of 10 cm at 0–100 cm, 20 cm at 100–300 cm and 40 cm at 320–980 cm. These disturbed soil samples were used for the determination of particle size distribution (PSD). The PSD was measured by laser diffraction using a Mastersizer 2000 and the determination of textural composition was based on USDA soil taxonomy. In addition to determining the percentage of clay, silt and sand content as well as median diameter (D_{50}), fractal dimension was used to evaluate the characteristics and variations of PSD. Fractal dimension integrates PSD information as well as the irregular shapes and self-similar structures of soils, and is determined by:

$$\frac{V(r < R_i)}{V_T} = \left(\frac{R_i}{\lambda_v}\right)^{3-D} \quad (2)$$

where $V(r < R_i)$ is the cumulative volume of soil particles with size r less than R_i, R_i is the particle diameter (mm) of the ith size class, V_T is the total volume of soil particles, λ_v is the diameter of the largest particle, and D is the fractal dimension of soil particles.

2.3.3. Soil water content

The SWC time series for volumetric water content consist of 113 readings ranging from July 2004 to September 2017. Without considering the duration days from spring green-up to autumn dormancy (Yang et al., 2015), the period from May to September between years was assumed to be the "growing season". During this time, the data was usually collected every one to two months. The SWC in the "non-growing season" was not regularly observed because it lacked variability. Growing season readings accounted for 66.4% of all readings.

The upper soil layer - to a certain depth - is strongly influenced by rainfall and evaporation, which varies greatly in different seasons and years. The SWC data within depth layers of 180–580 cm in 2004–2017 and 180–960 cm in 2014–2017 were employed in this study. Note that

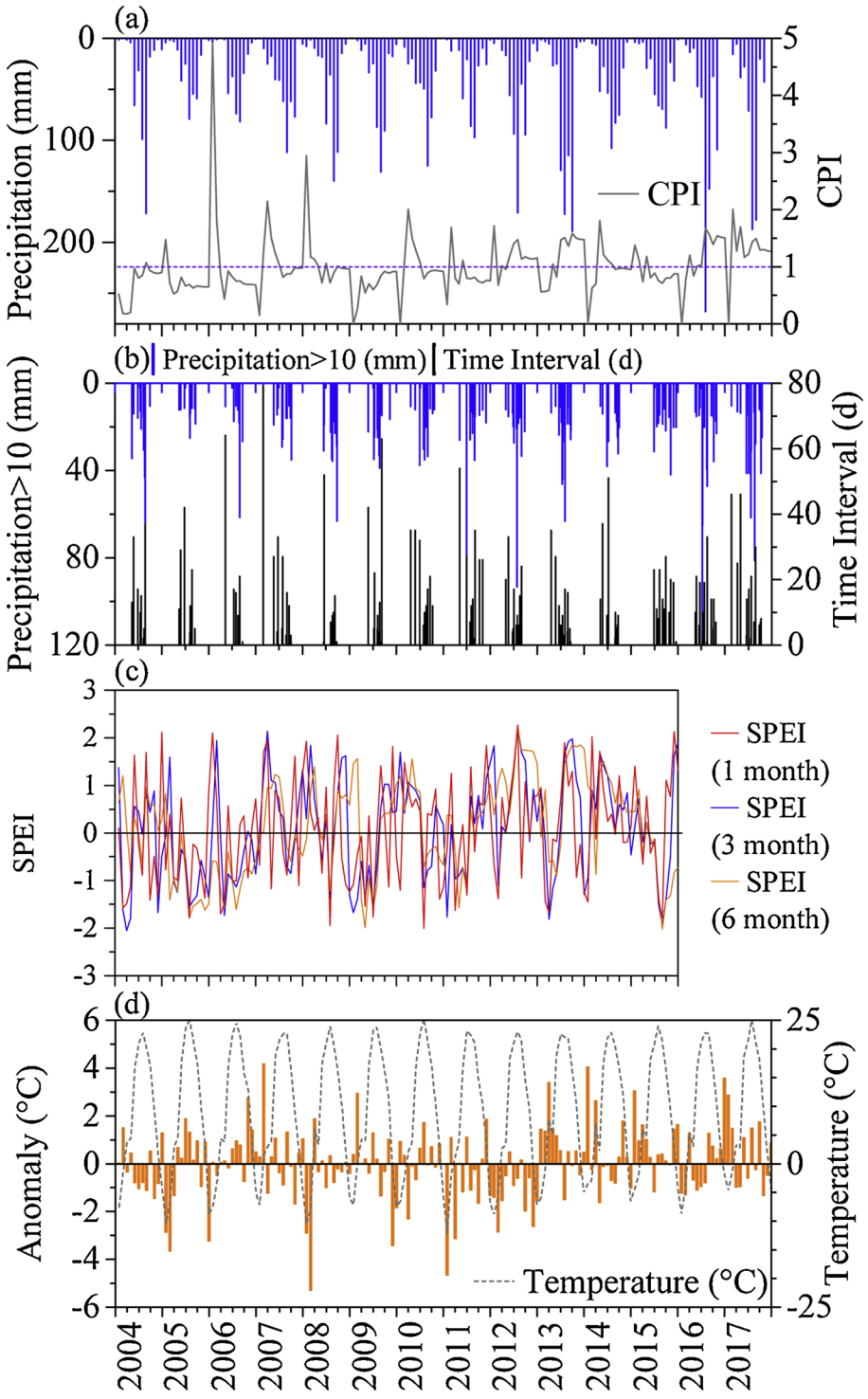

Fig. 2. In the period between 2014 and 2017, the monthly precipitation and cumulative precipitation index (CPI) are shown in image (a). The precipitation events of > 10 mm and the time interval (d) for every event are indicated in the image (b). The standardized precipitation evapotranspiration index (SPEI) at the timescale of 1, 3, and 6 months are shown in image (c), which ended in December 2015. Temperature and anomaly are shown in image (d).

0–180 cm soil depth, SWC were excluded to avoid the seasonal and inter-annual variation. Another reason for selecting these depths were that the available depth of the SWC between 2004 and 2014 was 580 cm, and it is common to calculate the mean SWC within a consistent depth of 100 cm. For example, the mean SWC within layers of 180–280 cm was the culmination of SWC at depths of 200, 220, 240, 260 and 280 cm averaged together. Moreover, soil water storage (SWS, mm) within certain depth layer was calculated by multiplying the volumetric SWC and its corresponding depth.

2.3.4. Identification of DSL and its descriptive parameters

The DSL was characterized as SWC lower than the stable field capacity (SFC) and distribution below the mean annual infiltration depth in the soil profile. Previous research concerned with the physiological response of plants (Yan et al., 2017) and indices have inconsistently quantified DSL severity (Li et al., 2008; Wang et al., 2018b). However, the SFC remains the most important criteria to judge whether DSL will occur. The SFC is highly dependent on soil texture (Shao et al., 2018) and equivalent to 50%–70% of the field capacity. The field capacity is

defined as volumetric SWC at −0.03 MPa, which is derived from soil water retention curve and based on the laboratory centrifugal test. In general, SFC is assumed to be 60% of the field capacity and simplified as a fixed value in the vertical soil profile (Dong et al., 2017; Wang et al., 2004a, b; Wang et al., 2011). In this study, 60% of the field capacity approximates 10.8% volumetric water content.

The depth range of soil affected by rainfall infiltration is about 1 − 3 m (Chen et al., 2008b). Allowing for the 14-year variation of annual precipitation amount, we set the value of mean annual infiltration depth to 200 cm for convenience during the calculations. Therefore, if a measured SWC was less than 10.8% at 220 cm depth, a DSL was considered to have formed and its formation depth was 200 cm. When SWC at multiple soil layers met the judgement criteria, the DSL thickness (DSLT) was calculated by multiplying the number of soil layers by the measurement interval of 20 cm. If the DSL was discontinuously distributed throughout the soil profile, the DSLT was obtained by adding up the thickness of every 20-cm DSL. The deepest depth of DSL in the soil profile was defined as the downward extension depth of DSL (DSL-DXD). The descriptive parameters also include DSL-SWC, which means soil water content inside DSL.

2.4. Statistical analysis

To describe the temporal trend of deep SWC in different soil layers, Mann-Kendall test, a non-parametric test for detection of monotonic trends in time series data, was performed. Prior to the Mann-Kendall test, the autocorrelation has been taken into account using the trend-free pre-whitening method (Yue and Wang, 2004). A positive value of Z indicates an upward trend while a negative value represents a downward trend. Pettitt's test (Pettitt, 1979) was used for evaluating the occurrence of abrupt changes for SWC time series.

To evaluate the differences of soil textural separates in the four plots, one-way analyses of variance followed by Duncan's multiple range test ($p < 0.05$) was used. On the basis of Pearson correlation among all selected climatic factors and SWC as well as DSL parameters, significant relationships were fitted with linear models. The variation of mean SWC with soil depth was evaluated with a linear regression. The relationship between DSLT and the Julian days since February 18, 2004, was fitted with a two-order polynomial function. A partial correlation analysis between SWC and the parameters of soil texture was performed.

3. Results and discussions

3.1. Background information of climatic change and soil texture

3.1.1. Climate change within the 14-year span

The annual precipitation during the 14-year observational period reached its lowest value of 298 mm in 2005 and highest value of 695 mm in 2016 (Fig. 2). These data exceeded the multiyear average in four years, including 2012, 2013, 2016, and 2017. The monthly precipitation during the growing and nongrowing seasons showed the average values of 77.18 and 10.84 mm, respectively; the former had a lower coefficient of variability than the latter (0.66 vs. 1.50). Sufficient precipitation during the nongrowing season may effectively recharge soil water. Meanwhile, low precipitation combined with high variability in precipitation will decrease the chance of DSL recovery.

The most lengthy interval of precipitation events > 10 mm occurred between March 3 and May 21 in 2007, which stood for a drought event with duration of 79 days. There were four precipitation events > 10 mm during the periods between April 21 and August 1 in 2010, and all had time intervals exceeding 30 days, which can be regarded as three drought events.

The API ranged between 0 and 193.45 mm, with < 50.9 mm accounting for 50%. The CPI in most months of the growing season had the values lower than 1. The CPI values of > 1 in the growing season mainly appeared in 2012, 2013, 2016, and 2017. From 2012 to 2014 and 2016 to 2017, the mean CPI values in the growing season were higher than those in the nongrowing season, and the opposite was observed from 2005 to 2008. In January 2005, the CPI reached its maximum value of 4.92 due to a heavy snowfall compared to the same month during the remaining observational years.

The monthly temperature varied from 14.51 °C to 25.32 °C in the growing season and from −12.19 °C to 13.00 °C in the nongrowing season; the latter had an extremely higher coefficient of variability than the former (0.14 vs. 9.48).

3.1.2. Textural information across the soil profiles

Previous studies conducted on the same plots as this study were based on the assumption of homogeneous soil texture at slope scale (Fu et al., 2012; Jia and Shao, 2014; Liu and Shao, 2015). The collection and analysis of soil samples in the deep vertical profiles in 2014 provided an opportunity to reveal the differences of the textural information among the four plots.

Two types of soil textures, that is, sandy loam and loamy sand, were identified in the vertical profiles of the four plots, and the proportion of sandy loam was far higher than that of loamy sand. The mean clay contents were 8.11%, 8.77%, 9.10%, and 9.73%, and the mean sand contents were 74.78%, 71.88%, 73.45%, and 70.29% in the KOP, ALF, NAF, and MIL plots, respectively. The interquartile ranges in ALF were the widest among the four plots (Fig. 3). The variance analysis results showed that the soil textural separates in KOP were significantly different from those in MIL ($p < 0.05$), and the soil profiles had high sand content in KOP and high clay content in MIL.

The fractal dimension of the PSD ranged from 2.382 to 2.509 in the KOP plot, with 62.5% of R^2 exceeding 0.90. In the ALF, NAF, and MIL plots, the fractal dimensions were in the ranges of 2.379–2.457, 2.407–2.519, and 2.066–2.475, with 65.6%, 78.1%, and 78.1% of the corresponding R^2 exceeding 0.90, respectively (Table 1). The fractal dimension performed well, as shown by the high R^2 values, which ranged from 0.88 to 0.95 in the KOP, ALF, and NAF plots and from 0.76 to 0.96 in the MIL plot. Overall, 96.1% of the fractal dimension values were within the range of 2.30–2.50. This result was consistent with the data range found in a previous study (Zhao et al., 2016), which reported soil profiles texture with a depth of 500 cm and PSD fractal dimension ranging from 2.13 to 2.69.

The median diameter (D_{50}) varied from 29.76 μm to 55.40 μm in ALF and 24.29 μm to 52.12 μm in MIL. The linear relationship between the D_{50} and fractal dimension in ALF and MIL was negative and significant, thereby indicating that finely textured soils tended to possess high fractal dimensions due to complete fragmentation. In response to a narrow D_{50} range, the relationship mentioned was insignificant in KOP

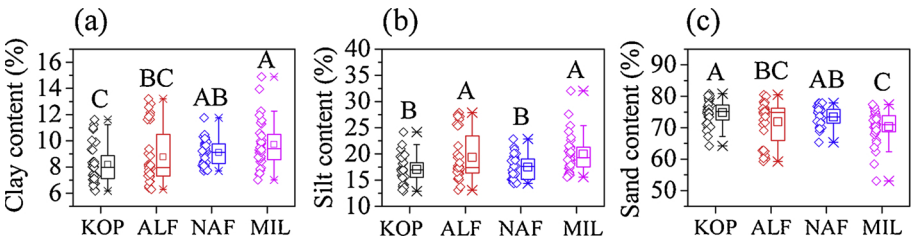

Fig. 3. Comparison of the soil textural separates in the four plots (i.e., KOP, Korshinsk peashrub; ALF, purple alfalfa; NAF, natural fallow; MIL, millet). The capital A, B, and C in the box chart indicate the significant difference at $p < 0.05$.

Table 1
The fractal dimension (FD) of soil particle size distribution and the median diameter ($D_{0.5,}$ um) at each soil depth in the four plots (KOP, ALF, NAF and MIL stand for revegetation types of Korshinsk peashrub, purple alfalfa, natural fallow and millet, respectively). R^2 is the coefficient of determination corresponding to the FD.

Depth	KOP			ALF			NAF			MIL		
	FD	R^2	$D_{0.5}$ (um)	FD	R^2	$D_{0.5}$ (um)	FD	R^2	$D_{0.5}$ (um)	FD	R^2	$D_{0.5}$ (um)
10	2.5091	0.93	47.90	2.431	0.9	50.54	2.4551	0.92	55.28	2.0663	0.76	52.118
30	2.4703	0.9	56.30	2.3888	0.9	48.19	2.5193	0.91	52.65	2.1547	0.82	47.931
50	2.4886	0.92	45.14	2.4082	0.88	55.40	2.4812	0.91	51.09	2.2887	0.9	50.386
70	2.4424	0.91	51.98	2.3791	0.9	52.21	2.4765	0.92	46.76	2.3948	0.94	44.274
90	2.4309	0.91	49.76	2.4123	0.9	52.63	2.4656	0.9	50.54	2.4639	0.92	45.547
120	2.4014	0.91	49.96	2.4104	0.9	53.54	2.465	0.89	52.43	2.4327	0.93	41.521
140	2.4083	0.91	51.00	2.4004	0.89	54.42	2.4317	0.91	50.15	2.4045	0.91	46.992
160	2.4216	0.91	52.74	2.4043	0.91	48.28	2.4334	0.93	40.87	2.4095	0.92	49.685
180	2.3847	0.92	50.10	2.4054	0.93	43.74	2.4074	0.92	46.91	2.4087	0.91	50.58
200	2.4166	0.9	56.03	2.4163	0.91	50.21	2.4927	0.91	55.05	2.4204	0.9	49.16
220	2.4212	0.9	56.67	2.4294	0.91	49.67	2.4591	0.91	53.12	2.4204	0.92	46.696
240	2.4093	0.89	56.93	2.4264	0.91	49.37	2.4422	0.9	53.87	2.4157	0.9	50.413
260	2.4205	0.9	55.00	2.401	0.91	49.90	2.4475	0.89	53.28	2.3973	0.9	50.821
280	2.3923	0.89	55.62	2.3859	0.9	51.44	2.4439	0.9	54.13	2.444	0.91	41.948
300	2.4198	0.89	56.44	2.3819	0.89	52.08	2.4517	0.9	51.96	2.4224	0.93	42.32
340	2.4379	0.92	51.11	2.418	0.91	48.99	2.4727	0.92	48.91	2.3901	0.92	40.413
380	2.4115	0.9	51.67	2.4207	0.93	46.65	2.4404	0.91	50.18	2.4244	0.93	46.246
420	2.3821	0.92	47.13	2.3957	0.89	47.08	2.4516	0.92	48.10	2.461	0.92	47.39
460	2.4304	0.92	51.41	2.4098	0.91	45.63	2.4654	0.93	44.87	2.419	0.91	44.217
500	2.4076	0.9	52.25	2.39	0.89	48.39	2.4284	0.91	49.15	2.4353	0.93	41.904
540	2.3876	0.91	49.57	2.3998	0.92	46.16	2.4404	0.92	45.82	2.4592	0.93	38.138
580	2.4057	0.92	47.44	2.4094	0.91	42.18	2.4283	0.92	45.20	2.4226	0.92	43.555
620	2.4212	0.91	46.59	2.4103	0.92	38.84	2.4316	0.9	50.02	2.4187	0.92	41.769
660	2.4081	0.9	46.34	2.4278	0.93	38.32	2.4317	0.91	46.79	2.4452	0.92	39.068
700	2.4301	0.9	47.76	2.4522	0.95	31.45	2.4647	0.92	42.93	2.4559	0.94	33.184
740	2.4036	0.9	43.95	2.4358	0.94	31.09	2.4171	0.92	40.54	2.4754	0.91	40.179
780	2.4345	0.92	43.97	2.4554	0.94	34.28	2.443	0.92	42.50	2.4398	0.9	43.903
820	2.4303	0.91	43.11	2.4562	0.95	29.76	2.4374	0.91	41.88	2.4504	0.92	35.318
860	2.4414	0.91	41.73	2.4453	0.94	36.58	2.4328	0.91	44.01	2.4406	0.91	38.661
900	2.4344	0.92	39.83	2.4543	0.95	30.09	2.4448	0.91	43.47	2.4455	0.92	33.173
940	2.4522	0.92	38.83	2.4554	0.94	35.18	2.4434	0.91	40.75	2.4696	0.94	28.753
980	2.4474	0.93	34.77	2.4573	0.94	35.74	2.4599	0.92	36.52	2.461	0.96	24.293

and positively significant in NAF.

3.2. Significant change in profile soil water due to revegetation

3.2.1. Overview of soil water deficit due to revegetation

For the upper 580 cm of the soil profile, the 14-year average SWC was compared with the initial SWC in July 2004 (Fig. 4). The SWS in KOP and ALF decreased by 123.26 and 166.57 mm within the depth layer range of 200–580 cm, respectively. The SWS in NAF and MIL decreased by 3 mm and increased by 44.41 mm, respectively. However, the time-averaged SWC, except for ALF, increased with the increase in depth (Fig. 5).

From 2014–2017, the soil water resources in KOP, ALF, NAF, and MIL, which were represented by the time-averaged SWS in the depth layers of 2–9.6 m, were 952.92, 1031.83, 1169.86, and 1367.91 mm, respectively. Taking the MIL plot as the control, the shrubs in KOP consumed 414.99 mm of soil water with a consumption rate, which was larger than that of the purple alfalfa in ALF (138.33 mm/a vs. 112.03 mm/a). According to the findings above, the SWC within the 600–960 cm layer was linearly correlated with soil depth. As reflected by the slope values (Fig. 5), the SWC in the same plot increased more rapidly in the lower 600 cm than in the upper 600 cm.

In terms of the plant morphological characteristics, ALF possessed an inherent advantage for soil recharge compared with KOP. The low leaf canopy density of ALF (Baldissera et al., 2013) was prone to rainfall reaching the ground, and its thick taproot created a space for preferential flow. In comparison, abundant branches and leaves of KOP intercepted a high proportion of rainfall (Yuan et al., 2017). However, the benefit of promoting infiltration in ALF was offset and even overpowered by the intensive water pump of *C. korshinskii* in most occasions.

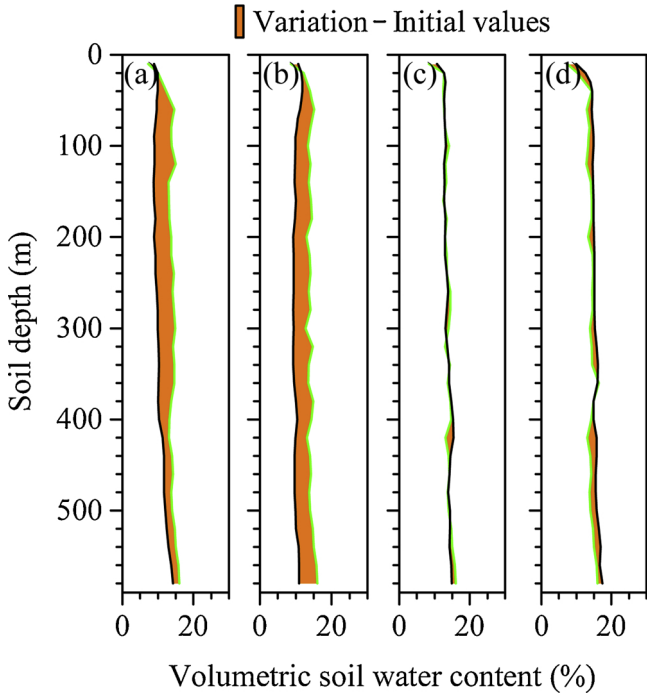

Fig. 4. Time-averaged variation of soil water content (SWC) in the vertical profiles in comparison with the initial values observed in July 2004. The plots of KOP, ALF, NAF, and MIL represent the revegetation types of Korshinsk peashrub, purple alfalfa, natural fallow, and millet, respectively. The SWC data within the 0–580 cm depth from 2004 to 2017 are presented in this figure.

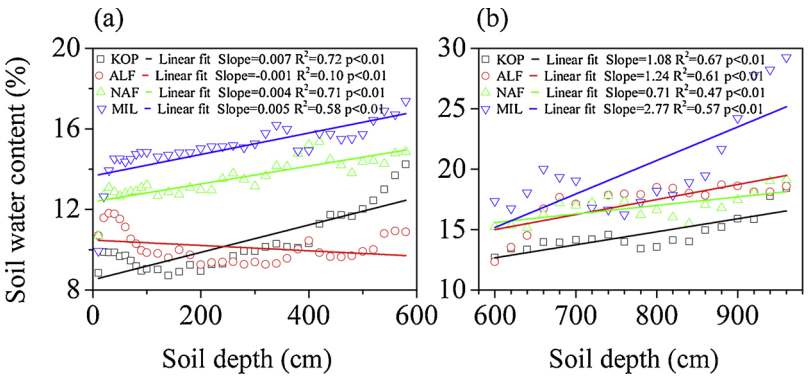
(a)
(b)
KOP – Linear fit Slope=0.007 R²=0.72 p<0.01
ALF – Linear fit Slope=-0.001 R²=0.10 p<0.01
NAF – Linear fit Slope=0.004 R²=0.71 p<0.01
MIL – Linear fit Slope=0.005 R²=0.58 p<0.01
KOP – Linear fit Slope=1.08 R²=0.67 p<0.01
ALF – Linear fit Slope=1.24 R²=0.61 p<0.01
NAF – Linear fit Slope=0.71 R²=0.47 p<0.01
MIL – Linear fit Slope=2.77 R²=0.57 p<0.01
Soil water content (%)
Soil depth (cm)
Soil depth (cm)

Fig. 5. Time-averaged soil water content (SWC) varies with observational depths. Image (a) shows the variation within soil depth of 0–580 cm between 2004 and 2017, and image (b) shows the variation within soil depth of 600–960 cm between 2014 and 2017. The linear regression results are also shown in the Figures. Four plots of KOP, ALF, NAF, and MIL stand for the revegetation types of Korshinsk peashrub, purple alfalfa, natural fallow and millet, respectively.

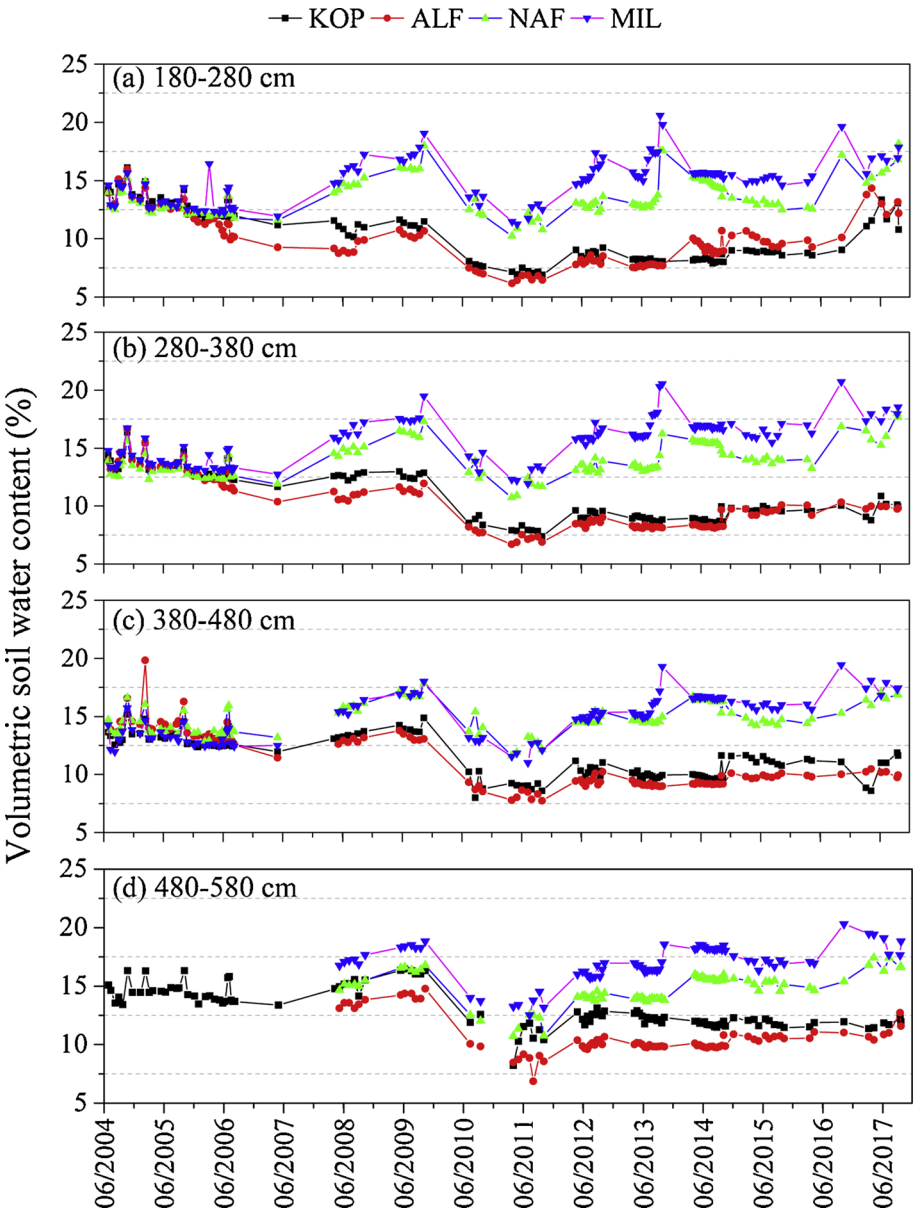

Fig. 6. Multiyear variation of mean SWC within the depth layers of 180–280 (a), 280–380 (b), 380–480 (c), and 480–580 cm (d) in the Korshinsk peashrub (KOP), purple alfalfa (ALF), natural fallow (NAF), and millet(MIL) plots, respectively.

3.2.2. Variation trend of profile SWC over 14 years

Using the 14-year accumulated SWC data in the four plots, Fig. 6 shows the temporal variation of the mean SWC at 180–280, 280–380, 380–480, and 480–580 cm. According to the shape of the curves, the mean SWC values in the different plots and soil layers had similar variation patterns with time. At the beginning of the experiment from 2004 to 2006, the SWC levels in the same soil layers were similar. However, the SWCs among different plots differed distinctly with time.

Table 2
Summary of trend analysis using Mann-Kendall test for mean soil water content (%) within four depth layers of each plot (Autocorrelations Method: Yue and Wang). The *Z*, β and *p* are Mann-Kendall statistics, significance level and Sen's slope, respectively. The unit of β is mm/*T*, *T* stands for the inconsistent time interval in this study. KOP, ALF, NAF and MIL stand for revegetation types of Korshinsk peashrub, purple alfalfa, natural fallow and millet, respectively.

Depth Layer	KOP			ALF			NAF			MIL		
	Z	*p*	β	*Z*	*p*	β	*Z*	*p*	β	*Z*	*p*	β
200-280 cm	137	0.662	0.003	953	**0.002**	0.S044	348	0.076	0.013	82	0.668	0.004
300-380 cm	−192	0.609	−0.006	253	0.479	0.009	620	**0.005**	0.022	750	< **0.0001**	0.021
400-480 cm	−296	0.346	−0.014	129	0.777	0.004	294	0.135	0.008	972	< **0.0001**	0.031
500-580 cm	−1188	< **0.0001**	−0.025	176	0.667	0.005	714	**0.001**	0.028	826	< **0.0001**	0.029

The temporal variation showed different peaks and troughs. The SWC peaks and troughs periodically alternated, thereby roughly keeping pace with the changes between the nongrowing and growing seasons. The peak values appeared in the nongrowing season and were concentrated in 2004–2005, 2008–2009, and 2016. Some peak values also appeared in the growing season, which occurred in 2006, 2010–2013, and 2017. The amplitude of the changes in SWC varied during the observational periods. These results can be associated with the plant species used for revegetation in the different plots, the interannual climate variability, and the vertical variability in soil texture.

Trend analysis by using the Mann–Kendall test was applied to the time series of the SWC, and the results are shown in Table 2. Given that the time intervals were nonuniform among the 113 measurements, some analyses were excluded (i.e., Sen's slope). Positive *Z* values at 180–280 cm were observed in all four plots. However, only one significantly increasing trend of SWC was detected in ALF, and its variation trend differed from that of the revegetation plant species. Decreasing trends represented by the negative *Z* values were detected in the three other soil layers in KOP. The smallest negative *Z* value at 480–580 cm indicated the steepest decline in SWC. The significance level ($p < 0.0001$) and the small Sen's slope ($\beta = -0.025$) both supported this result. Thus, the soil water within this depth layer is most strongly consumed in KOP compared with those at 280–380 and 380–480 cm. The *Z* values in ALF, NAF, and MIL were all positive, with the half of the number of depth layers significant at $p < 0.005$, thereby indicating an increasing trend in SWC in the corresponding soil layers. The increase in SWC can be linked to rainfall infiltration, storage, and its subsequent surplus. The *Z* value in ALF was at its maximum in the uppermost soil layer, thereby indicating the evident occurrence of rainfall recharge within the 180–280 cm depth layer. The soil water in the layers below 280 cm was more replenished in NAF and MIL than in KOP and ALF. In KOP, the decrease in soil water occurred in 180–280 cm, while the SWC decreased to < 280 cm, which suggests that rain can also infiltrate the 180–280 cm depth and is unconsumed by *Caragana korshinskii*. One possible explanation for this result is that the soil water replenishment mainly resulted from the concentrated infiltration of rainfall in the nongrowing season.

3.2.3. Change point detection for SWC time series

The differences in the abrupt increases and decreases of SWC occurred in the four plots despite all plots being under the same climatic conditions, as shown by the analysis of the change point detection by using Pettitt's test (Fig. 7). For the SWC at 180–280 cm, abrupt increases in ALF and NAF, an abrupt decrease in KOP, and no abrupt change in MIL were observed. These results confirmed the profound effects of revegetation species on the vertical distribution of SWC. An abrupt decrease in SWC mainly occurred on the same date (October 20, 2009). By contrast, the abrupt increase mainly occurred at different and continuous measurement times in 2013. These results were partially explained by the amount and frequency of precipitation events of > 10 mm. In 2009, precipitation events > 10 mm occurred three times between September and November, with the total value of 45.3 mm. However, in September 2013, the precipitation events of > 10 mm occurred four times, with the total value of 78 mm.

Compared with the upper three soil layers in KOP, a long delay in the abrupt decrease in SWC occurred at 480–580 cm on October 17, 2013. This phenomenon can be linked to the soil water uptake ability of *C. korshinskii* at different ages. Under soil water stress, older plant ages may correspond to a considerable downward extension of plant roots. For the abrupt increase in SWC that occurred in NAF, the change points in adjacent depth layers were continuous. The four continuous downward depth layers were observed on September 2, September 17, October 2, and October 17 in 2013. These results can be explained by the time lag of the infiltration, which also reflected the infiltration capacity of rainfall in the vertical soil profiles.

3.3. DSL formation, evolvement, and replenishment

3.3.1. Plant-induced DSL and its trajectory

In terms of SFC, no DSL emerged in the soil profiles at the beginning of plot establishment. This phenomenon began to change in KOP and ALF with the increase in plant growth years (Fig. 8). On February 18, 2006, during the nongrowing season, the DSL was identified at 200–240 cm. The same DSL thickness in KOP was observed on May 9, 2007 when the *C. korshinskii* was 4 years old. This result proved that the DSL in the soil profile can be the consequence of revegetation on SWC. Early-stage alfalfa had a stronger ability to transpire water than aged *C. korshinskii*, and two consecutive years of growing alfalfa triggered the formation of a DSL. Under a 2-year-old alfalfa grassland, Li (1983) found that DSL began to form below the 210 cm depth and then extended to 480 cm in the 3rd year. Wang et al. (2010b) found that the DSL was thicker after growing alfalfa for 4 years than that after growing *C. korshinskii.* In the present study, from 2006 to 2017, except for few months, the DSL in ALF was consistently thicker than that in KOP.

When alfalfa grew for 7 years and *C. korshinskii* for 8 years, the DSL induced by their growth reached the maximum DXD. This phenomenon occurred quickly in KOP because DXD took < 1 year (from October 20, 2009 to July 22, 2010) to shift from 240 cm to 460 cm. The process of DSL extension to 580 cm was comparatively gradual in ALF. This contrast can be linked to the larger biomass of *C. korshinskii* than that of alfalfa, which may lead to a distinct difference in transpiration amounts, especially when the fast-growing stage became out of sync for the two species.

For KOP and ALF, a change point on the basis of Pettitt's test for the DSL thickness time series occurred on July 22, 2010, wherein the DSLT was 260 cm in KOP and 380 cm in ALF. The abrupt increase in DSLT was linked to water depletion by the vegetation during the period of rapid growth. Three drought events respectively lasted over 30 days also contributed to such a result. The abrupt increase in DSLT occurred later than the abrupt decrease in SWC (which occurred on October 20, 2009). This result indicated that the variation of DSLT was slower than the change in DSL-SWC.

During the entire observation period, the DSL-DXD varied from 220 cm to 580 cm. In comparison, the DSLT in ALF was relatively stable, ranging from 200 cm to 380 cm, after the occurrence of the maximal value. Yan et al. (2015) reported that the DSLT under alfalfa

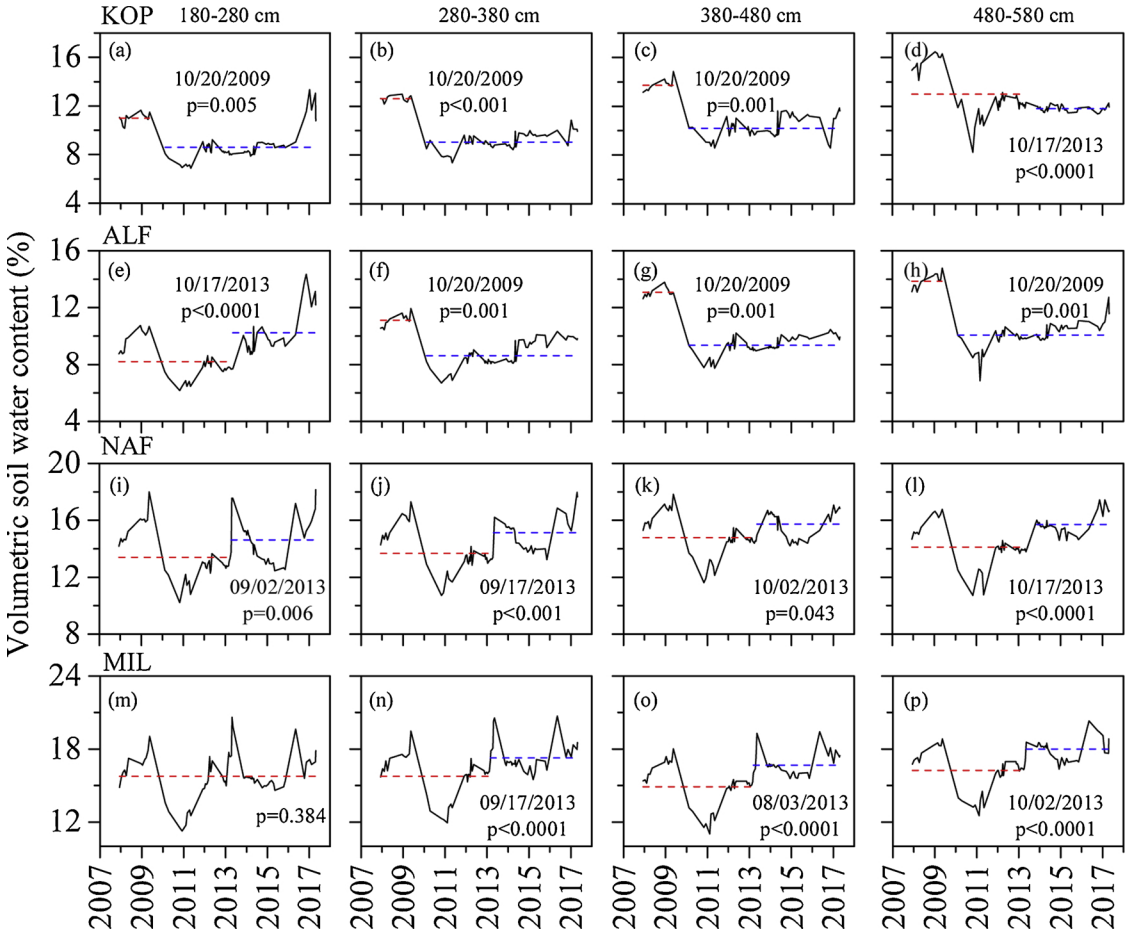

Fig. 7. Change point detection by using Pettitt's test for mean soil water content within four depth layers (180–280, 280–380, 380–480, and 480–580 cm) in the four plots (KOP, Korshinsk peashrub; ALF, purple alfalfa; NAF, natural fallow; MIL, millet).

grassland can reach 1000 cm after growing for 8 years and exceed 2000 cm after growing for 23 years. However, the maximal DSLT of alfalfa in the present study did not extend downward when the planting years increased from 8 to 14 (Fig. 8). The relationship between DSLT and Julian days was best fitted with two-order polynomial functions, and the corresponding coefficient of determination in ALF was higher than that in KOP (Fig. 9). This result implied that the thickness of DSL varied nonlinearly with the growth time of plants. Compared with ALF, the curve tail in KOP was close to the baseline of 2007 when the DSL first emerged in the plot. Yan et al. (2015) reported a long-term relationship between DSLT and planting years (> 30 years), but no decreasing trend was exhibited in the fitted curve. The discrepancy between their study and our study can be partially linked to the different methodologies and data sources used. Yan et al. (2015) used meta-analysis and synthesized discontinuous results in different experiments, whereas the results in the present study were based on the consecutive observations of the same experiment plots. Another possible reason is that the wet year coincides to the degradation of vegetation. There is no doubt that the relatively concentrated occurrence of wet year would substantially slow down the development of DSL. However, we did not observe the vegetation degradation in the experimental plots.

The mean DSL-SWC in ALF was smaller than that in KOP (9.26% vs. 9.32%). The fluctuation of DSL-SWC suggested the existence of soil water movement inside the DSL. The upper DSL can be replenished because the formation depth once ranged from 220 cm to 320 cm in KOP and from 220 cm to 300 cm in ALF (Fig. 10). The formation depth dynamics of DSL was linked to the thinning of the DSL from its upper surface. The deep DSL tended not to recover following its formation.

A dramatic drop of DSLT in KOP occurred in 2017 when the DSLT decreased from a high value of 3.0 m to the minimum of 0.8 m. However, an increasing trend was observed in the DSLT between 2014 and 2016. A similar phenomenon also occurred in ALF, where the DSLT averaged 3.2 m between 2014 and 2016 but decreased to 2.2 m in 2017. The DSLT decline resulted from soil replenishment within the previous DSL, which was a positive signal for soil water resources threatened by DSL. The 30-day antecedent precipitation before October 16, 2016 was 93.3 mm. Nearly no plant water consumption occurred in the non-growing season. Thus, for the next period, considerable amount of the infiltrated water had high possibility of moving to the deep soil layers. Before and after 2017, the mean formation depth of DSL changed from 2 m to 2.6 m in KOP and from 2.1 m to 2.9 m in ALF. The maximal formation depths of DSL were 3.2 and 3.0 m in KOP and ALF, respectively. These results suggested the alleviation of the upper DSL. Through a simulated rainfall experiment conducted on the hillslope of Changwu county, Chen et al. (2008a) found that most infiltrated rainwater moves to the 0–300 cm soil layer. It is speculated that plant-induced DSL may impede the moisture movement in the soil profile, and the possibility of water reaching the soil below 2 m depth is small. Our results indicated that under natural condition, when heavy rainfall occurred late in the year, especially in October, deep infiltration increased and thinned the DSL.

3.3.2. *Phenomenon of sandwiched DSL*

A phenomenon that has not been reported is that DSL and non-DSL were alternatively distributed in the deep vertical soil profiles (Fig. 10). For example, in KOP, the DSL within 460–480 cm starting on July 20, 2012 was followed by alternating DSL-non-DSL occurrences over time and again between December 14, 2014 and October 16, 2016. The

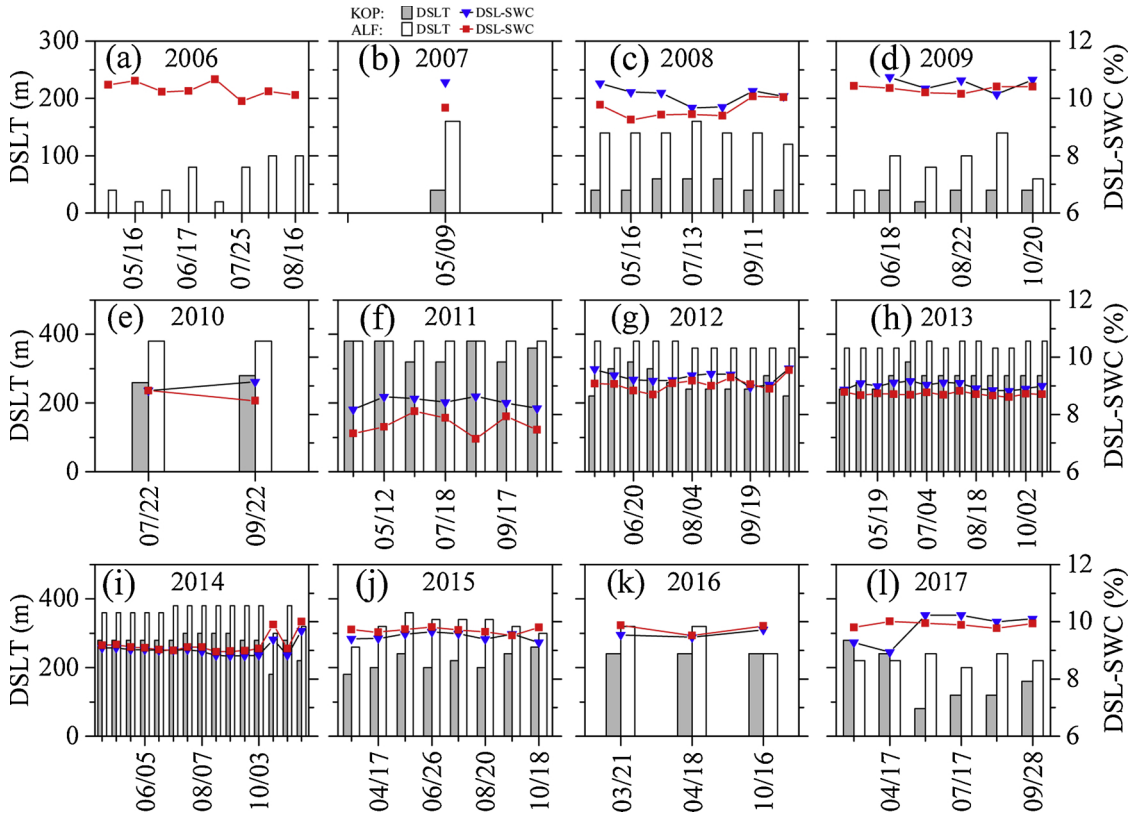

Fig. 8. Quantitative description of the formation and evolvement of plant-induced dried soil layers (DSL) in the vertical profiles of Korshinsk peashrub (KOP) and purple alfalfa (ALF). The DSLT and DSL-SWC stands for the DSL thickness (cm) and soil water content within DSL (%), respectively.

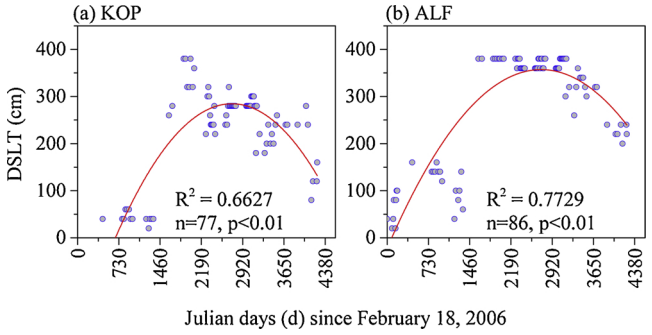

Fig. 9. Two-order polynomial relationship between the Julian days since February 18, 2016 and the DSLT in both plots of KOP and ALF.

thickness of the DSL situated between two non-DSLs in time in KOP varied, but the frequency of 20 cm thick DSL occurred 61.5% of the time (Fig. 11). The short-lived DSL that was sandwiched between two non-DSLs tended to disappear following recharge. However, a thick sandwiched DSL will persist for a long time. One sandwiched DSL that was 260 cm thick occurred below the 220 cm depth in KOP on March 17, 2017, which existed within depth of 260–460 cm on April 17, 2017. Afterward, the thick sandwiched DSL was partitioned into discontinuous fragments in the soil profile. Thus, DSL thinning may occur from the intermittent recharge under a moisture gradient. This phenomenon indicated that the thicker the sandwiched DSL is, the lower the possibility of full recharge will be. This finding was consistent with that of Jia et al. (2015), who considered that DSL with a thick DSLT possesses considerably strong temporal persistence.

The thickness of sandwiched DSL ranged from 20 cm to 320 cm in ALF, and the greatest DSL frequency was 20 cm, which occurred 25.8% of the time. The thickest sandwiched DSL of 320 cm occurred on four observational occasions, as follows: April 21, May 21, and December 14 in 2014 and April 17, 2015. Rough comparisons with KOP suggested that the sandwiched DSL in ALF stretched to a thick depth and had low opportunity to be replenished. Accompanied with sandwiched DSL, sandwiched non-DSL was also observed. The highest frequency of non-DSL thickness corresponded to 20 cm, which were 47.1% and 88.9% of the time in KOP and ALF, respectively. Note that the frequency and extent of sandwiched DSL and non-DSL also depended on the identification criteria of DSL.

The sandwiched DSL was directly linked to the process of moisture transfer in DSLs. A sandwiched DSL reflects the flexibility of DSL evolvement and is an indicator of the possibility of DSL thinning. The identification of non-DSL sandwiched between DSLs can be considered as a snapshot of DSL disappearance, which was in progress, and the recovery of the DSL remains uncertain. The phenomenon of sandwiched non-DSL verified that the occurrence of DSL did not completely block moisture movement, and the DSL can be alleviated and reclaimed.

3.4. Quantitative evaluation of climate and soil texture effects

3.4.1. Bidirectional effect of wet climate on DSL

Overall, the climatic data from the growing season performed better than the nongrowing season in terms of explaining the effects of climatic factors on SWC and DSL according to the Pearson correlation results (not shown). Thus, the subsequent analysis is derived mainly from the climatic data in the growing season (Fig. 12).

In both KOP and ALF, the monthly precipitation showed a significantly negative relationship with SWC at 180–280, 280–380, and 380–480 cm, which indicated that the soil tended to be water-deficient under conditions of rainwater supply. On one hand, a small amount of rainwater cannot enter the soil. On the other hand, this negative relationship may be caused by the small amount of initially recharged soil water that did not satisfy the increasing demand of plants. The newly added infiltrated water was not stored in soil as it was used by

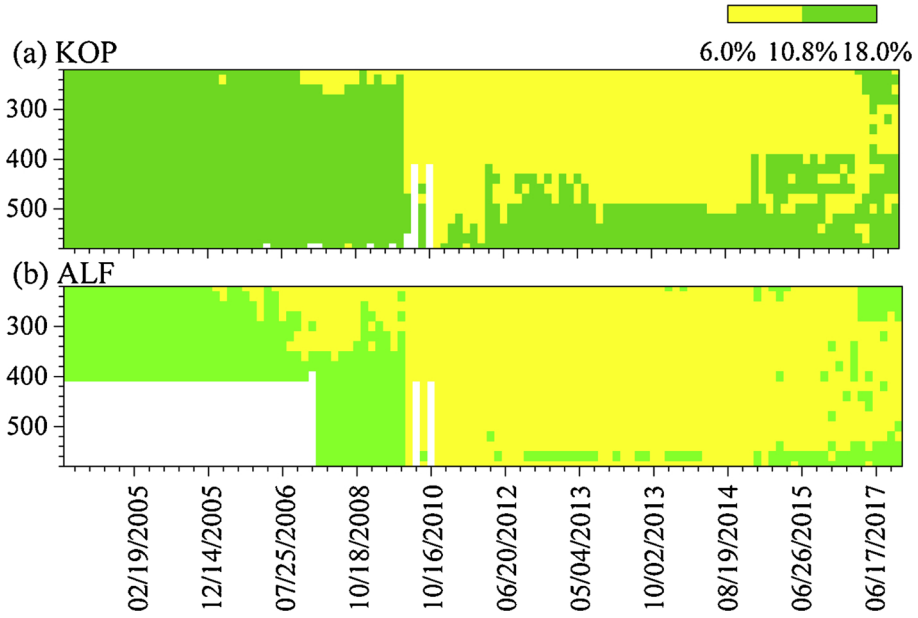

Fig. 10. Sandwiched phenomenon of DSL (dried soil layer) between non-DSLs. In the soil profiles of Korshinsk peashrub (KOP) and purple alfalfa (ALF), the yellow zone indicates DSL, the green zone depicts non-DSL, and the blank zone represents the lack of observation in the past experiment.

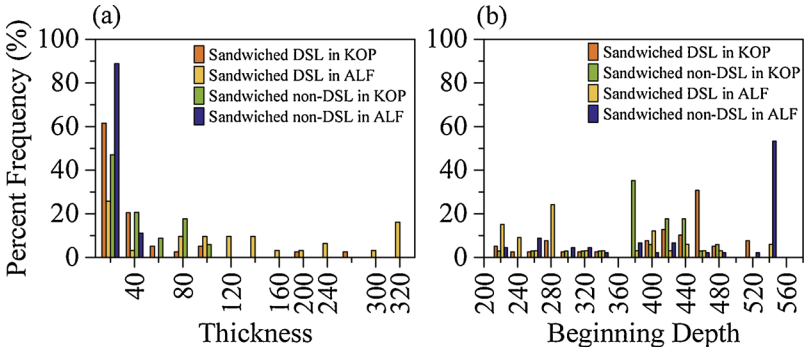

Fig. 11. Percent frequency of thickness (a) and beginning depth (b) of the sandwiched dried soil layer (DSL) and non-DSL in Korshinsk peashrub (KOP) and purple alfalfa (ALF).

vegetation, which is an adaptive strategy of plants under condition of DSL development. In the growing season, the water-consuming potential of plants under considerable water supply will be triggered and promoted by plant transpiration. The plants in KOP and ALF consumed both the newly added and the previously stored water in soil and depleted the soil water resources. No similar results were found in NAF and MIL, which supported the statement above to a certain extent.

The positive relationship between SPEI and DSLT strengthened with the increased length of the timescale. When the selected SPEI timescale was 1, 3, and 6 months, the correlation coefficients increased both in KOP and ALF. The positive relationship was also significant ($p < 0.01$) in ALF when the SPEI timescale was 3 and 6 months. These results indicated that the thickening of DSL benefited from long-term wet climate conditions, which corresponded to a high SPEI value. As shown in Fig. 12, the DSL-DXD and DSLT in ALF increased with the increase in SPEI. A SPEI of 6 months was superior to that of 3 months in explaining the DSL variability on the basis of the significant linear relationship. The linear relationship of temperature anomalies against DSL-SWC in ALF was significantly positive. In KOP, the enhancement of CPI will also aggravate the DSL status, as shown in Fig. 12g-h. In both KOP and ALF, the development of DSL was promoted under wet climate conditions, thereby indirectly indicating the predominant role of vegetation transpiration in the evolvement of DSL and decrease in SWC.

The wet climate was linked to both DSL thinning and thickening, which provided a robust explanation for DSL deep beneath the land surface. Wang et al. (2013) reported that DSL occurred within 21 m profiles at 11 sites across the Loess Plateau. Wang et al. (2009) identified the DSL at a deep soil and considered that 7-year-old alfalfa and 23-year-old *C. korshinskii* peashrub depleted soil water at the depths of 15.5 and 22.4 m, respectively. In a symposium, Professor Yushan Li, who is the pioneer of DSL research, indicated that old deep DSLs under croplands occurred before it was reclaimed for farming (Li, 2015). We tended to believe the process was slow for DSL development in the deep soil profile. A favorable climate with high SPEI as well as positive temperature anomalies facilitated vegetation growth, partly contributed to the extraordinary development of DSL in the deep soil profile. It is also worth noting that we did not deny the positive role of drought climate in promoting DSL occurrence in the early stage. But in the long term, the wet climate conditions during the growing season delay the degradation process of plants and provide possibility for DSL expansion, while drought conditions may retard its continual development by inhibiting plant growth. Thus, the effect of climate change on DSL development is bidirectional, which also implies the decisive role of revegetation.

3.4.2. SWC sensitivity to textural variation

To explore the effect of soil texture on SWC in the vertical soil profiles, we performed a partial correlation analysis between SWC and

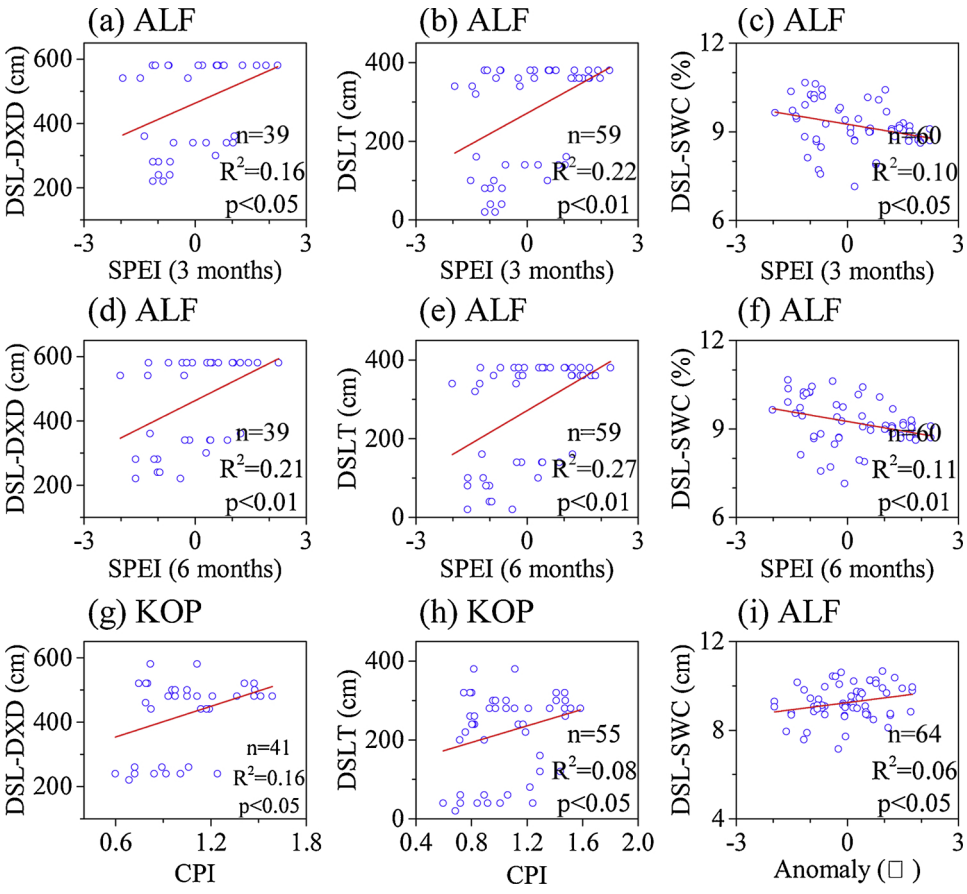

Fig. 12. Significant linear relationships between climate factors and the parameters of dried soil layer (DSL) in the Korshinsk peashrub (KOP) and purple alfalfa (ALF) plots. SPEI and CPI stand for the standardized precipitation evapotranspiration and cumulative precipitation indices, respectively. DSL-DXD, DSLT and DSL-SWC stand for the downward extension depth, the thickness of DSL, and the mean soil water content of DSL, respectively.

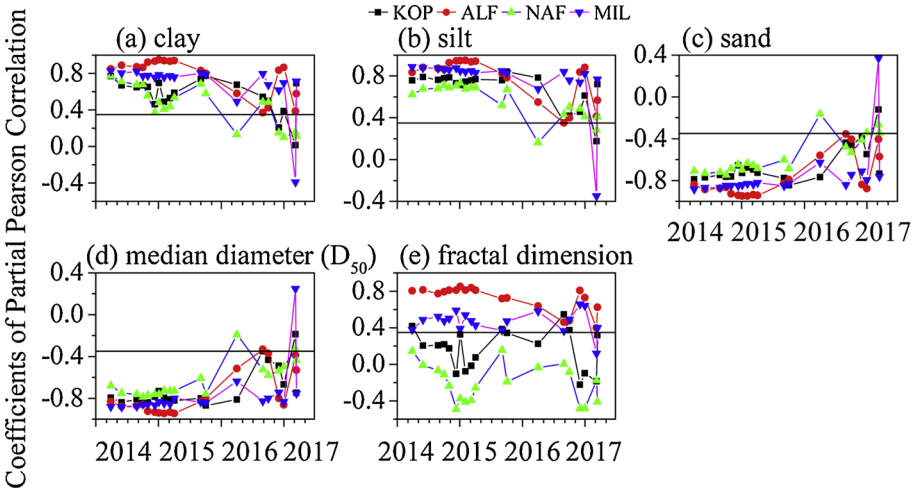

Fig. 13. Varying soil water content (SWC) sensitivity to soil texture in the vertical soil profiles with time. The coefficients of the partial correlation between SWC and the parameters of soil texture are the surrogates of SWC sensitivity to textural variation. The images of (a)–(e) use the soil textural parameters of clay, silt, and sand percent (%), the median diameter (D_{50}, um), and the fractal dimension, respectively.

the parameters of soil texture for each plot (Fig. 13). The coefficient of correlation fluctuated with time, and was a surrogate of SWC sensitivity to textural variation.

In most observational occasions, SWC had a positive correlation with clay and silt content and a negative correlation with sand content and D_{50} at either $p < 0.05$ or $p < 0.10$. The correlations were all significant in ALF. Insignificant correlations mainly appeared on two dates, namely, October 16, 2016 and September 23, 2017. Both dates corresponded to possible chances of soil water recharge. On October 16, 2016, the insignificant correlation appeared only in NAF. We speculated that the DSL in ALF and the high clay soil led to the stability of SWC sensitivity to textural variation. The increase in DSL thickness on May 16, 2015 in KOP and ALF corresponded to a decrease and increase of its sensitivity, respectively, compared with that on April 17, 2015. This result can be partially explained by the relative differences in soil texture. On September 23, 2017, the decrease in the DSL thickness in KOP and the substantial replenishment of soil water resources under sandy soil in NAF disrupted the SWC sensitivity to textural variation. This result showed that the effect of profile soil texture on SWC may be stenohydric. In most cases, the sensitivity of SWC to soil texture was significant. However, in the special cases of deep soil water recharge and DSL thinning in the vertical profile, although the SWC sensitivity to textural variation was present, the effects of soil texture on SWC were decreased.

The correlation between fractal dimension and SWC can also describe the effects of soil texture on SWC in ALF and MIL instead of in

KOP and NAF. This result indicated that the fractal dimension was not as effective as other selected parameters in defining SWC sensitivity to textural variation.

4. Conclusion

On the basis of a consecutive observation of plant-induced DSL, we determined whether DSL was temporary or persistent and the extent of its relationship with exotic perennial plants, climate factors, and soil texture. Revegetation with *C. korshinskii* and alfalfa distinctly affected the variation trends of the SWC profile and triggered the formation of DSL. The downward extension of DSL even reached a depth of 580 cm. Direct evidence for the possibility of DSL recovery, including the formation depth dynamics of DSL, the fluctuation of soil moisture inside the DSL, and the phenomenon of sandwiched DSL, was proposed. Wet climate had bidirectional behavior on DSL, besides, the decisive role of revegetation in DSL development was determined. The findings on DSL formation and evolvement and the relevant mechanism will improve our understanding of soil desiccation in China's Loess Plateau.

Authors contributions

Yuhua Jia and Tongchuan Li contributed equally in planning and writing the manuscript, as well as in data collection. Ming'an Shao contributed to the general design and support. Jianhui Hao and Yunqiang Wang participated in the discussion, and Xiaoxu Jia reviewed the manuscript. Ceng Zeng, Xiaoli Fu, Bingxia Liu, and Mingyang Zhao all contributed to the long-term data collection. Miao Gan and Xinni Ju contributed to the formulation of the equation and by taking pictures with a drone, respectively.

Acknowledgements

This work was supported by the National Natural Science Foundation of China (41390463, 41571221, 41571130081, 41601216) and the State Key Laboratory of Soil Erosion and Dryland Farming on the Loess Plateau (A314021402-1504). Many thanks go to Fang-Ling Hu and Xiao-Guang Tang for their help on language check.

References

Baldissera, T.C., Frak, E., Carvalho, P.Cd.F., Louarn, G., 2013. Plant development controls leaf area expansion in alfalfa plants competing for light. Ann. Bot. 113 (1), 145–157.
Chen, H., Shao, M., Li, Y., 2008a. The characteristics of soil water cycle and water balance on steep grassland under natural and simulated rainfall conditions in the Loess Plateau of China. J. Hydrol. 360 (1–4), 242–251.
Chen, H., Shao, M., Li, Y., 2008b. Soil desiccation in the Loess Plateau of China. Geoderma 143 (1), 91–100.
Chen, Y., et al., 2015. Balancing green and grain trade. Nat. Geosci. 8 (10), 739–741.
Dong, S., Li, T., Guo, C., Jia, Y., Jin, S., 2017. Distribution of dried soil layers on the dividing waterline in the gully area of the Loess Plateau (in Chinese). Adv. Water Sci. 28 (6), 811–819.
Feng, X., Fu, B., Lu, N., Zeng, Y., Wu, B., 2013. How ecological restoration alters ecosystem services: an analysis of carbon sequestration in China's Loess Plateau. Sci. Rep. 3, 2846. https://doi.org/10.1038/srep02846.
Feng, X.M., et al., 2016. Revegetation in China's Loess Plateau is approaching sustainable water resource limits. Nat. Clim. Chang. 6 (11), 1019–1022.
Fu, X., Shao, M., Wei, X., Wang, H., Zeng, C., 2012. Effects of monovegetation restoration types on soil water distribution and balance on a hillslope in Northern Loess Plateau of China. J. Hydrol. Eng. 18 (4), 413–421.
Fu, B., et al., 2016. Hydrogeomorphic ecosystem responses to natural and anthropogenic changes in the Loess Plateau of China. Annu. Rev. Earth Planet. Sci. 45 (1), 223–243.
Gan, M., Jia, Y., Shao, Ma., Guo, C., Li, T., 2019. Permanent gully increases the heterogeneity of soil water retention capacity across a slope-gully system. Agric. Ecosyst. Environ. 272, 206–217.
Gao, X., et al., 2017. Temporal and spatial evolution of the standardized precipitation evapotranspiration index (SPEI) in the Loess Plateau under climate change from 2001 to 2050. Sci. Total Environ. 595, 191–200.
Gong, T., Zhu, Y., Shao, Ma., 2018. Spatial distribution of caliche nodules in surface soil and their influencing factors in the Liudaogou catchment of the northern Loess Plateau. China. Geoderma 329, 11–19.
Green, J.C., Reid, I., Calder, I.R., Nisbet, T.R., 2006. Four-year comparison of water contents beneath a grass ley and a deciduous oak wood overlying Triassic sandstone in lowland England. J. Hydrol. 329 (1), 16–25.
Huang, M., Yang, X., Li, Y., 2003. Hydro-ecological effect of the soil dry layer as affected by biota use in the Loess Plateau (in Chinese). Chin. J. Eco-Agric. 11 (3), 113–116.
Jia, Y.-H., Shao, M.-A., 2013. Temporal stability of soil water storage under four types of revegetation on the northern Loess Plateau of China. Agric. Water Manag. 117, 33–42.
Jia, Y.-H., Shao, M.-A., 2014. Dynamics of deep soil moisture in response to vegetational restoration on the Loess Plateau of China. J. Hydrol. 519, 523–531.
Jia, Y.-H., Shao, M.-A., Jia, X.-X., 2013. Spatial pattern of soil moisture and its temporal stability within profiles on a loessial slope in northwestern China. J. Hydrol. 495, 150–161.
Jia, X., Shao, Ma., Zhu, Y., Luo, Y., 2017. Soil moisture decline due to afforestation across the Loess Plateau, China. J. Hydrol. 546, 113–122.
Jiao, J., Zhang, Z., Bai, W., Jia, Y., Wang, N., 2012. Assessing the ecological success of restoration by afforestation on the Chinese Loess Plateau. Restor. Ecol. 20 (2), 240–249.
Jipp, P.H., Nepstad, D.C., Cassel, D.K., Carvalho, C.R.D., 1998. Deep soil moisture storage and transpiration in forests and pastures of Seasonally-Dry Amazonia. Clim. Change 39 (2-3), 395–412.
Li, Y., 1983. The properties of water cycle in soil and their effect on water cycle for land in the Loess Region (in Chinese). Acta Ecol. Sin. 3 (2), 91–101.
Li, Y., 2015. Soil Water Cycle and Farmland Productivity (in Chinese). Shaanxi People's Publishing House, Xi'an.
Li, J., et al., 2008. Effects of deep soil desiccation on artificial forestlands in different vegetation zones on the Loess Plateau of China. Acta Ecol. Sin. 28 (4), 1429–1445.
Liang, W., et al., 2015. Quantifying the impacts of climate change and ecological restoration on streamflow changes based on a Budyko hydrological model in China's Loess Plateau. Water Resour. Res. 51 (8), 6500–6519.
Liu, B.X., Shao, M.A., 2014. Estimation of soil water storage using temporal stability in four land uses over 10 years on the Loess Plateau, China. J. Hydrol. 517, 974–984.
Liu, B., Shao, M.A., 2015. Modeling soil–water dynamics and soil–water carrying capacity for vegetation on the Loess Plateau, China. Agric. Water Manag. 159 (2), 176–184.
Ma, L.-h., Liu, X.-l., Wang, Y.-k., 2013. Effects of drip irrigation on deep root distribution, rooting depth, and soil water profile of jujube in a semiarid region. Plant Soil 373 (1-2), 995–1006.
Miralles, D.G., Teuling, A.J., Van Heerwaarden, C.C., de Arellano, J.V.-G., 2014. Megaheatwave temperatures due to combined soil desiccation and atmospheric heat accumulation. Nat. Geosci. 7 (5), 345–349.
Pettitt, A., 1979. A non-parametric approach to the change-point problem. Appl. Stat. 28 (2), 126–135.
Robinson, N., Harper, R.J., Smettem, K.R.J., 2006. Soil water depletion by Eucalyptus spp. Integrated into dryland agricultural systems. Plant Soil 286 (1-2), 141–151.
Samaniego, L., et al., 2018. Anthropogenic warming exacerbates European soil moisture droughts. Nat. Clim. Chang. 8 (5), 421–426.
Seneviratne, S.I., Lüthi, D., Litschi, M., Schär, C., 2006. Land–atmosphere coupling and climate change in Europe. Nature 443 (7108), 205–209.
Shangguan, Z., 2007. Soil desiccation occurrence and its impact on forest vegetation in the Loess Plateau of China. Int. J. Sustain. Dev. World Ecol. 14 (3), 299–306.
Shao, Ma., Jia, X., Wang, Y., Zhu, Y., 2016. A review of studies on dried soil layers in the Loess Plateau (in Chinese). Adv. Earth Sci. 31 (1), 14–22.
Shao, Ma., Wang, Y., Xia, Y., Jia, X., 2018. Soil drought and water carrying capacity for vegetation in the critical zone of the Loess Plateau: a review. Vadose Zone J. 17 (1). https://doi.org/10.2136/vzj2017.04.0077.
Tang, K.L., Hou, Q.C., Wang, B.K., Zhang, P.C., 1993. The environment background and administration way of wind—water erosion crisscross region and Shenmu experimental area on the Loess Plateau (in Chinese). Res. Soil Water Conserv. 2, 1–14.
Tye, A., Lawley, R., Ellis, M., Rawlins, B., 2011. The spatial variation of weathering and soil depth across a Triassic sandstone outcrop. Earth Surf. Process. Landf. 36 (5), 569–581.
Vicente-Serrano, S.M., Beguería, S., López-Moreno, J.I., 2010. A multiscalar drought index sensitive to global warming: the standardized precipitation evapotranspiration index. J. Clim. 23 (7), 1696–1718.
Wang, D., Wang, L., 2018. Soil water dynamics in apple orchards of different ages on the Loess Plateau of China. Vadose Zone J. 17 (1), 180049. https://doi.org/10.2136/vzj2018.03.0049.
Wang, L., Shao, M., Hou, Q., 2001. The primary research on dried soil layer in the Loess Plateau. J. Northwest A&F Univ. (Nat. Sci. Ed.) 29 (4), 34–38.
Wang, L., Shao, M., Wang, Q., Jia, Z., Li, J., 2004a. Review of research on soil desiccation in the Loess Plateau. Trans CSAE 20 (5), 27–31.
Wang, L., Shao, M., Zhang, Q., 2004b. Distribution and characters of soil dry layer in north Shaanxi Loess Plateau (in Chinese). Chine. J. Appl. Ecol. 15 (3), 436–442.
Wang, Y., Shao, Ma., Liu, Z., 2010a. Large-scale spatial variability of dried soil layers and related factors across the entire Loess Plateau of China. Geoderma 159 (1), 99–108.
Wang, Y., Shao, Ma., Shao, H., 2010b. A preliminary investigation of the dynamic characteristics of dried soil layers on the Loess Plateau of China. J. Hydrol. 381 (1), 9–17.
Wang, Y., Shao, Ma., Zhu, Y., Liu, Z., 2011. Impacts of land use and plant characteristics on dried soil layers in different climatic regions on the Loess Plateau of China. Agric. For. Meteorol. 151 (4), 437–448.
Wang, S., et al., 2016. Reduced sediment transport in the Yellow River due to anthropogenic changes. Nat. Geosci. 9 (1), 38–41.
Wang, S., Fu, B., Chen, H., Liu, Y., 2018a. Regional development boundary of China's Loess Plateau: water limit and land shortage. Land Use Policy 74, 130–136.
Wang, Y., Shao, Ma., Zhu, Y., Sun, H., Fang, L., 2018b. A new index to quantify dried soil layers in water-limited ecosystems: a case study on the Chinese Loess Plateau. Geoderma 322, 1–11.

Wu, G.L., et al., 2016. Mosaic-pattern vegetation formation and dynamics driven by the water-wind crisscross erosion. J. Hydrol. 538, 355–362.
Yan, W.M., Deng, L., Zhong, Y.Q.W., Shangguan, Z.P., 2015. The characters of dry soil layer on the Loess Plateau in China and their influencing factors. PLoS One 10 (8), e0134902. https://doi.org/10.1371/journal.pone.0134902.
Yan, W., Zhong, Y., Shangguan, Z., 2017. Responses of different physiological parameter thresholds to soil water availability in four plant species during prolonged drought. Agric. For. Meteorol. 247, 311–319.
Yang, Y., Guan, H., Shen, M., Liang, W., Jiang, L., 2015. Changes in autumn vegetation dormancy onset date and the climate controls across temperate ecosystems in China from 1982 to 2010. Glob. Chang. Biol. 21 (2), 652–665.
Yuan, C., Gao, G., Fu, B., 2017. Comparisons of stemflow and its bio-/abiotic influential factors between two xerophytic shrub species. Hydrol. Earth Syst. Sci. 21 (3), 1421–1438.
Yue, S., Wang, C., 2004. The Mann-Kendall test modified by effective sample size to detect trend in serially correlated hydrological series. Water Resour. Manag. 18 (3), 201–218.
Zeng, C., Shao, M., Wang, Q., Zhang, J., 2011. Effects of land use on temporal-spatial variability of soil water and soil-water conservation. Acta Agric. Scand. Sect. B–Soil Plant Sci. 61 (1), 1–13.
Zhang, S., et al., 2018. Excessive afforestation and soil drying on China's Loess Plateau. J. Geophys. Res. Biogeosci. 123 (3), 923–935.
Zhao, C., Shao, Ma., Jia, X., Zhang, C., 2016. Particle size distribution of soils (0–500cm) in the Loess Plateau, China. Geoderma Regional 7 (3), 251–258.
Zhao, C., Jia, X., Zhu, Y., Shao, Ma., 2017. Long-term temporal variations of soil water content under different vegetation types in the Loess Plateau, China. CATENA 158, 55–62.
Zhou, G., et al., 2011. Quantifying the hydrological responses to climate change in an intact forested small watershed in Southern China. Glob. Chang. Biol. 17 (12), 3736–3746.
Zhu, Y., Jia, X., Shao, M., 2018. Loess thickness variations across the Loess Plateau of China. Surv. Geophys. 39 (4), 715–727.